Frustration in smectic layers of polar Gay-Berne systems

W. Józefowicz* and L. Longa†

Marian Smoluchowski Institute of Physics, Department of Statistical Physics and Mark Kac Center for Complex Systems Research, Jagellonian University, Reymonta 4, Kraków, Poland

(Received 27 March 2007; published 11 July 2007)

The main focus of the present paper is studying dipolar frustration within smectic-A_d layers as induced by dipole-dipole interactions. Our reference point is the Gay-Berne system with $\kappa=4$, $\kappa'=5$, $\mu=2$ and $\nu=1$, which in the phase diagram shows a stable "island" of smectic-*A* phase with a short-range hexagonal order within each layer [Phys. Rev. E **57**, 6685 (1998)]. We carry out isothermal-isobaric Monte Carlo simulations for a dipolar version of this model, where the Gay-Berne interaction is supplemented by interaction between longitudinal dipole moments. For a fixed off-center position of the dipoles we increase value of the dipole moment and follow evolution of the liquid-crystalline part of the phase diagram focusing on changes of the nematic-smectic-*A* phase boundaries and on structural response of the smectic-*A* layers. For weak dipoles only the classical smectic-*A* phase is stabilized, which then transforms into smectic-A_d with layers being formed by two ferroelectrically polarized sublayers of opposite polarization. Average positions of dipoles that contribute to the polarization of a sublayer are located in a common plane, referred to as a dipolar plane. For not too strong dipole-dipole interactions increasing magnitude of the dipole moment causes stabilization of nematic at the expense of smectic-A_d. Under the same conditions the layer spacing increases and the distance between the dipolar planes within layers decreases. Each smectic sublayer is characterized by a short-range hexagonal order of the molecular centers of mass. With the dipole moment exceeding the threshold value, the polarization planes that built up the layers start to merge, which sets in the dipolar frustration. This, in turn, forces the system to develop a competition between frustrated hexagonal- and frustration-free tetragonal local order within each layer. When the local hexagonal order is transformed into the tetragonal one the stability range of smectic-A_d increases with increasing dipole moment at the expense of the nematic phase. Similar competition is observed in crystalline phases. For small dipole moment only crystalline structures with long-range hexagonal order appear stable. They evolve with dipolar strength into monoclinic and tetragonal lattices.

DOI: 10.1103/PhysRevE.76.011701 PACS number(s): 61.30.−v, 64.70.Md, 05.10.Ln

I. INTRODUCTION

When antiferroelectrically interacting Ising spins reside on a two dimensional triangular lattice locally favorable antiparallel spin configurations cannot be extended globally to fill in the space. As an immediate consequence of this is a macroscopic degeneracy of the ground state of the system and the absence of long-range order even at zero absolute temperature. Wannier, in his seminal paper of 1950 [1], was able to quantify this observation and the effect, later on, coined the name frustration. Today various manifestations and importance of frustration are demonstrated for magnetic systems, neural networks, structural glasses, biomatter, or liquid crystals [2]. Among these examples liquid crystals form a special group of materials, where the structure not only can dictate the behavior through frustration but, itself, can respond to it. As a result, unexpected patterns can emerge among which the blue phases of cholesteric liquid crystals are one example [3]. Another is the rich smectic *A* polymorphism and reentrant phase transitions observed in systems with strong longitudinal dipole moments [4]. The layer spacing of these smectic phases ranges from l to $2l$, where l is the molecular length. Some of them build up layers consisting of polarized sublayers with, on average, opposite direction of the dipoles (smectic-A_d and smectic-A_2 phases), or a striped dipolar structure (smectic-$\tilde{A}$ phase).

These observations inspired several theoretical studies, which sought to explain the precise rôle dipolar forces can play in stabilizing liquid crystalline phases [5,6] and, especially, polar smectics [7]. But the progress has been relatively slow, mainly because of inherent difficulty in treating dipole-induced, many-body correlations by density functional theories. Such higher than binary correlations should be taken into account for a proper understanding of the dipole-induced frustration. Indeed, consider nematic or smectic-A phases with locally preferred hexagonal ordering of molecular centers of mass, the case we will be dealing with in this paper. Under these circumstances two longitudinal dipole moments attain their energetically most stable configuration in an antiparallel arrangement. When we consider a third dipole approaching the other two dipoles, we note that it does not find any favorable orientation: being antiparallel to one it must be parallel to the other, which is the energetically least stable configuration for two dipoles. We say that the three-dipole configuration of liquid crystalline molecules becomes frustrated in a precisely the same way as the three nearest-neighbor Ising spins become frustrated on the Wannier's lattice [1]. An important difference between the two situations, however, is that an ensemble of dipoles in a *fluid state* can respond to the frustration by seeking for a more optimal structural arrangement, which is not possible for the rigid lattice of Ising spins. Clearly, nature of

*wjozefow@th.if.uj.edu.pl
†longa@th.if.uj.edu.pl

this response is enforced by frustrated configurations involving three- and more molecules and, hence, three- and higher particle correlations are crucial here. A direct and reliable way to look into these correlations are computer simulations.

From a theoretical perspective, it is natural to study the problem of frustration in smectic-*A* layers from relatively simple models for which the case of vanishing dipole is well understood and contains stable structures of interest. In this regard a remarkably successful model is a pair potential as developed by Gay and Berne (GB) [8]. The GB potential is the single-site, anisotropic generalization of the standard 12-6 Lennard-Jones interaction to molecules of uniaxial symmetry. It depends on the unit vectors $\hat{\mathbf{e}}_i$ and $\hat{\mathbf{e}}_j$ describing the orientations of a pair of molecules and on the separation vector $\mathbf{r}_{ij}=\mathbf{r}_i-\mathbf{r}_j$ of their centers of mass $\mathbf{r}_i$ and $\mathbf{r}_j$. The detailed expression is given by

$$V_{\mathrm{GB}}(\hat{\mathbf{e}}_i,\hat{\mathbf{e}}_j,\mathbf{r}_{ij}) = 4\epsilon(\hat{\mathbf{e}}_i,\hat{\mathbf{e}}_j,\hat{\mathbf{r}}_{ij})(R^{-12}-R^{-6}), \tag{1}$$

where

$$R = [r_{ij} - \sigma(\hat{\mathbf{e}}_i,\hat{\mathbf{e}}_j,\hat{\mathbf{r}}_{ij}) + \sigma_0]/\sigma_0. \tag{2}$$

Here $r_{ij}=|\mathbf{r}_{ij}|$ is the length of the separation vector, $\hat{\mathbf{r}}_{ij}=\mathbf{r}_{ij}/r_{ij}$ is its orientation. Explicit expressions for the orientation-dependent molecular shape parameter σ and the anisotropic energy parameter ϵ may be found in the original paper by Gay and Berne [8]. They depend on $\hat{\mathbf{e}}_i$, $\hat{\mathbf{e}}_j$, and $\hat{\mathbf{r}}_{ij}$, as well as on six parameters (κ,κ',μ,ν) and $[\sigma_0,\epsilon_0(\epsilon \sim \epsilon_0)]$. The four parameters (κ,κ',μ,ν) control the anisotropy of the repulsive and attractive forces while the last two introduce a natural length and energy scale. The parameters κ and κ' are the length-to-width ratio and the potential well depths ratio for the side-to-side and end-to-end arrangements, respectively, while the parameters μ and ν tune details of the well depth shape. The pair (σ_0,ϵ_0) corresponds to the shape parameter and well depth calculated for a cross configuration, where three molecular vectors $\hat{\mathbf{e}}_i$, $\hat{\mathbf{e}}_j$, and $\hat{\mathbf{r}}_{ij}$ are mutually perpendicular.

The GB model has been extensively analyzed with the help of molecular dynamics and Monte Carlo (MC) simulations. It owes its remarkable success to a rich liquid crystalline polymorphism obtained for various selections of (κ,κ',μ,ν) [9–13]. In addition, the model also predicts a phase behavior that agrees well with what is observed for real mesogens. For example, the most thoroughly documented case with $\kappa=3$, $\kappa'=5$, $\mu=2$ and $\nu=1$ reveals isotropic liquid, nematic, and crystalline smectic-*B* phases [9]. In view of this success the original model has been extended further to include such important characteristics of liquid crystalline molecules as biaxiality, flexibility, or distribution of localized charges. In particular, the dipole-dipole approximation of interactions between the charges resulted in extensive simulation investigations of polar GB potentials. A concise overview is found in a recent paper by one of us [14]. As concerning frustration-induced formation of structures some of the results for polar GB systems with longitudinal dipoles are of interest. In particular, Longa *et al.* [15] have analyzed a system of perfectly oriented polar Gay-Berne particles and have identified stable smectic A_d and tetragonal crystalline phases with smectic A_d and A_2-like dipolar organization for various localizations and strengths of the dipole. Berardi *et al.* have found a stable smectic-$\tilde{A}$ phase for terminal dipoles [16] and a smectic-A_d phase at intermediate dipole location (i.e., between terminal and central position) [17] in case when full spectrum of rotational degrees of freedom has been allowed for a polar GB. Their paper [17] shows the effect of dipole strength on the transformation from smectic-*A* to smectic-A_d structures.

The present paper is focused on a systematic constant-*NPT* MC simulations (constant number of particles, pressure and temperature) of polar GB systems with longitudinal dipoles. Our goals encompass investigation of the evolution of the liquid-crystalline part of the phase diagram with increasing value of the dipole moment and studies of the system's response to the dipolar frustration through structural properties. As a reference nonpolar GB system we select one with parameters $\kappa=4$, $\kappa'=5$, $\mu=2$, and $\nu=1$, extensively studied by Brown *et al.* [12] and hereafter referred to as BARM. It shows isotropic phases (*I*), nematic phase (*N*), a stable "island" of smectic-*A* phase (with a short-range hexagonal order of the molecular centers of mass within the layers) and crystalline smectic-*B* phase (*AB* stacking). BARM is therefore an ideal candidate for studying frustration-induced structural reorganization of smectic-*A* and crystalline phases.

We equip each GB molecule with an embedded longitudinal dipole moment, placed on a molecular symmetry axis not far away from the molecular center of mass, which (as it turns out) allows to observe the frustration-induced competition between hexagonal- and tetragonal order, both in smectic-A_d and crystalline phases. Also we follow the evolution of the liquid-crystalline part of the phase diagram with increasing value of the dipole moment. Structure analysis is given in terms of one-particle distribution and two- and three-particle correlation functions. In particular, we demonstrate that three-particle correlations are of particular importance for a proper understanding of the dipolar frustration.

The present paper is arranged as follows. After introduction of the model and computational details in Sec. II, we explore the evolution of liquid crystalline part of the phase diagram with increasing value of the dipole moment in Sec. III. Using the results of the latter section, we perform fine structure analysis of the smectic-A_d in-layer correlations in Sec. IV. A purpose of these studies is to clarify the rôle played by frustration. Section V is devoted to a short summary.

The parameters σ_0 and ϵ_0 of the GB potential provide a natural length and energy scale for the system. In terms of these parameters all relevant physical quantities studied in this paper, also referred to as reduced quantities, are rendered dimensionless. Their definitions are found, e.g., in Appendix A of [15]. To keep notation simple we omit asterisk, usually associated with names of the reduced quantities.

II. MODEL AND SIMULATION DETAILS

We consider prolate uniaxial molecules with point dipole moments parallel to the molecular symmetry axis. The pair interaction between molecules *i* and *j* is defined as

$$V = V_{\mathrm{GB}}\Theta(R_c - r_{ij}) + V_{dd}, \tag{3}$$

where V_{GB} is the Gay-Berne potential (1) with BARM parameters $\kappa=4$, $\kappa'=5$, $\mu=2$, and $\nu=1$; Θ is the Heaviside function. V_{dd} represents the dipole-dipole interaction due to permanent longitudinal dipole moments $\boldsymbol{\mu}_i=\mu\hat{\mathbf{e}}_i$, placed along the main symmetry axis of the Gay-Berne molecule

$$V_{dd}(\mathbf{r}_{ij},\hat{\mathbf{e}}_i,\hat{\mathbf{e}}_j) = \frac{\mu^2}{\rho_{ij}^3}[\hat{\mathbf{e}}_i\cdot\hat{\mathbf{e}}_j - 3(\hat{\boldsymbol{\rho}}_{ij}\cdot\hat{\mathbf{e}}_i)(\hat{\boldsymbol{\rho}}_{ij}\cdot\hat{\mathbf{e}}_j)]. \tag{4}$$

Here $\boldsymbol{\rho}_{ij}=\mathbf{r}_{ij}+d_s(\hat{\mathbf{e}}_i-\hat{\mathbf{e}}_j)$ is the relative separation between dipole moments of the two GB molecules, $\hat{\boldsymbol{\rho}}_{ij}=\boldsymbol{\rho}_{ij}/\rho_{ij}$, d_s is the distance of the dipole from the molecular center of mass and μ is the dipole moment value (not to be confused with one of the GB parameters). In all the work presented here the dipole is positioned at $d_s=0.5$ and the GB potential is truncated at $R_c=5.0$. Defined as above, the GB part of the interaction potential slightly differs from the one studied by Brown *et al.* [12] in that we have dropped the shift term that makes the GB potential vanish at R_c. We have carried out a few test simulations confirming that our results are consistent with the diagram presented in [12]. Considering differences our triple point of isotropic-nematic-smectic is at higher temperature (i.e., $T=1.1$ instead of $T=1.0$ [12]) and the liquid-crystal–crystal hysteresis is more pronounced. This latter feature is probably also due to the larger system size, i.e., 1000 instead of 600 particles studied in [12].

The dipole-dipole interaction, due to its long range nature, requires special treatment in computer simulations [19]. Usually either a direct, but expensive, molecule-molecule Ewald summation technique is used or its relatively cheap molecule-continuum counterpart, known as Onsager reaction-field method. We used the reaction field method, which amounts in replacing $V_{dd}(\mathbf{r}_{ij},\hat{\mathbf{e}}_i,\hat{\mathbf{e}}_j)$ in Eq. (4) by $V_{dd}^{\mathrm{RF}}(\mathbf{r}_{ij},\hat{\mathbf{e}}_i,\hat{\mathbf{e}}_j)$ [14,19,20], where

$$V_{dd}^{\mathrm{RF}} = \left[V_{dd} + \frac{2\mu^2(1-\epsilon_{RF})}{(1+2\epsilon_{RF})}\frac{\hat{\mathbf{e}}_i\cdot\hat{\mathbf{e}}_j}{R_c^3}\right]\Theta(R_c-\rho_{ij}). \tag{5}$$

The static dielectric constant ϵ_{RF}, which represents the medium outside the cutoff sphere of radius R_c, should be calculated self-consistently so that the average dielectric constant of the simulation box agrees with ϵ_{RF}. But in practice the simulations are often carried out with $\epsilon_{RF}=\infty$ (tin-foil value) [14,19,20], which was also our choice in the present simulations, or with finite values [17]. For structures with vanishing *average* dipole moment of the central box the numerical value of ϵ_{RF} does not affect, within error, calculated thermodynamic properties. This has been explicitly demonstrated for the Stockmayer fluid [21] in liquid and vapor phases, and for the dipolar Gay-Berne systems with longitudinal dipole moments, where selfconsistent, tin-foil and finite values of ϵ_{RF} have been used [15,20,22,23]. Importantly, the results for the dipolar Gay-Berne ensembles agreed with results obtained by applying the Ewald summation technique [15,17,22].

We performed extensive constant-*NPT* Monte Carlo simulations for relatively large system of $N=1000$ molecules confined to a tetragonal box and subjected to the periodic boundary conditions and minimum image convention [19]. A Monte Carlo move consisted of trial displacement and reorientation of a molecule at constant volume, a trial flip of the dipole moment orientation ($\boldsymbol{\mu}_i\rightarrow-\boldsymbol{\mu}_i$), and an attempted volume move realized by sampling independently the mutually orthogonal box sides. The parameters controlling maximal increment of the displacements and the orientations were adjusted during simulation to guarantee the acceptance rate for the combined move between 10% and 50%. The acceptance rate for the dipole flips was chosen 30% and for volume changes was kept between 10% and 60%. Low acceptance rates were especially important for dense, highly ordered states allowing partly to overcome the metastability traps. The number of cycles needed to equilibrate the system ranged from 5×10^5 up to 10^6. The production run took another 10^5 cycles with particle configurations being saved every 10 cycles for a subsequent analysis of distribution functions. We studied behavior of the system along isotherms starting from low temperatures. For each temperature we initialized simulations in the isotropic liquid phase at low pressures and slowly increased pressure (compression) until a transformation to a highly ordered "crystalline" phases has been achieved. Then we decreased pressure all the way back (decompression) to the same isotropic phase. The runs for dense systems were also complemented by simulations initiated from crystalline ground state configurations, obtained for $T=0$ by a direct minimization of the potential energy (see Table I and Fig. 9). The total number of all state points simulated for each isotherm varied between 20 and 40. In the liquid crystalline part of the phase diagrams points, which approximate a phase boundary at given temperature (diamonds in Fig. 8) are the last stable points obtained before transition into more ordered (less ordered) phase took place on compression (decompression). The area between these points approximates the corresponding coexistence region. Downward triangles, connected by a dashed line in Fig. 8, mark points where a crystalline phase undergoes a transition into a liquid-crystalline one on decompression. We were unable, however, except for a few isolated points, to determine the corresponding line on compressing the system from a liquid crystalline to crystalline phase due to large hysteresis effects. Similar difficulties were reported by de Miguel and Vega [9]. Hence the phase boundaries between liquid crystalline and crystalline phases can only be regarded as tentative.

III. STRUCTURE ANALYSIS AND PHASE DIAGRAMS

In this section we report on studies of the polar GB fluid, where the reduced dipole moment increased in steps of 0.5 ($0.5\leq\mu\leq2.5$). Our simulations run along five isotherms of the reduced temperatures: $T=(1.0,1.1,1.25,1.4,1.5)$ and additionally, for $T=1.05$. Except for isotropic, nematic and smectic-A_d phases the system stabilizes crystalline phases with the corresponding ground states given in Table I. In some cases more than one stable crystalline phase has been detected for a single isotherm. Below is a presentation of the phases obtained for different values of the dipole moment along with the corresponding evolution of the liquid crystal-

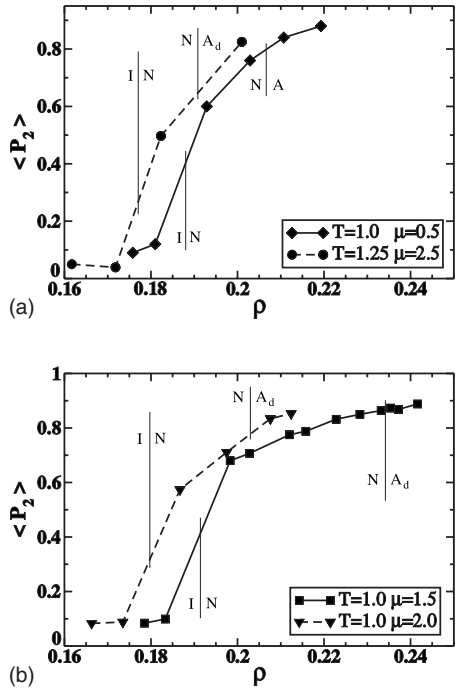

FIG. 1. Density dependence of orientational order parameter $\langle P_2 \rangle$ for exemplary values of reduced dipole moment μ and reduced temperatures T across different phases.

line part of the phase diagram. Structure analysis essentially follows that described in two papers by one of us [14,15]; brief summaries will be given when appropriate. Full account of technical details concerned with simulations is found in [12,14,15,19].

The isotropic-to-nematic phase transition is monitored using the standard second-rank tensor order parameter, defined as

$$\mathbf{\Omega} = \frac{1}{2N}\left\langle \sum_{i=1}^{N} (3\hat{\mathbf{e}}_i \otimes \hat{\mathbf{e}}_i - \mathbf{1}) \right\rangle, \tag{6}$$

where N is the number of particles in the simulation box and $\langle \cdots \rangle$ is the isobaric-isothermal ensemble average. The largest eigenvalue of this tensor gives the average value of the second Legendre polynomial, $\langle P_2 \rangle$, the leading orientational order parameter of liquid crystals; the corresponding eigenvector defines the director $\hat{\mathbf{n}}$. Evolution along isotherms of the orientational order parameter with density for exemplary values of the dipole moment is shown in Fig. 1. It turns out that $\langle P_2 \rangle$ is high both in nematic ($\langle P_2 \rangle \geq 0.5$) and smectic-$A_d$ phases ($\langle P_2 \rangle \geq 0.8$) for the isotherms studied. In addition, all structures found show no sign of ferroelectric, long-range order. That is the average value of the first-rank Legendre polynomial $\langle P_1 \rangle = (1/N)\langle \Sigma_i \hat{\mathbf{n}} \cdot \hat{\mathbf{e}}_i \rangle$ vanishes within error.

Positional long-range order along the director was searched for with the help of longitudinal, one- and two-particle distribution functions. Since the orientational order parameter in smectic-A_d and "crystalline" phases was found high we quantified the dipolar order of the molecules using the discrete variable $s_i = \pm 1$, such that $s_i = +1 \equiv \uparrow$ for $\boldsymbol{\mu}_i \cdot \hat{\mathbf{n}} > 0$ and $s_i = -1 \equiv \downarrow$ for $\boldsymbol{\mu}_i \cdot \hat{\mathbf{n}} < 0$. That is, we divided population of the dipole moments into two subsets, one containing dipoles pointing towards positive direction of the z-axis and the other with dipoles pointing down. For the director aligned along the z-axis, which we assume henceforth, the dipolar ordering along the director was probed with the one-particle distribution function, defined as

$$P^{(1)}(z,s) = \frac{\overline{L_z}}{N}\left\langle \sum_{\alpha=1}^{N} \delta_{s\, s_\alpha} \delta(z - z_\alpha) \right\rangle, \tag{7}$$

where $s = \pm 1$, $\overline{L_z}$ is the reduced average length of the simulation box along $\hat{\mathbf{z}}$ and z_i is the zth reduced coordinate of the "i"-th particle. $P^{(1)}(z,s)$ is composed of two polarization waves of opposite polarizations, which we denote $P^{(1)}(z,\uparrow)$ and $P^{(1)}(z,\downarrow)$, respectively. It reads

$$P^{(1)}(z,s) = \frac{1}{2}[P^{(1)}(z,\uparrow) + P^{(1)}(z,\downarrow)] + \frac{s}{2}[P^{(1)}(z,\uparrow) - P^{(1)}(z,\downarrow)]. \tag{8}$$

As the average polarization of the system along the z-axis vanishes $[\Sigma_{s=\pm 1}(1/\overline{L_z})\int_0^{\overline{L_z}} s P^{(1)}(z,s)dz = 0]$, the functions $P^{(1)}(z,\uparrow)$ and $P^{(1)}(z,\downarrow)$ must fulfill the normalization condition:

$$\frac{1}{\overline{L_z}}\int_0^{\overline{L_z}} P^{(1)}(z,\uparrow)dz = \frac{1}{\overline{L_z}}\int_0^{\overline{L_z}} P^{(1)}(z,\downarrow)dz = \frac{1}{2}. \tag{9}$$

In addition, they are periodic functions of period d, shifted with respect to each other by a distance Δ, both in smectic-A_d and crystalline phases. That is

$$P^{(1)}(z,\uparrow) = P^{(1)}(z+d,\uparrow), \tag{10}$$

$$P^{(1)}(z,\downarrow) = P^{(1)}(z+d,\downarrow), \tag{11}$$

$$P^{(1)}(z,\downarrow) = P^{(1)}(z+\Delta,\uparrow). \tag{12}$$

Associated with the distribution functions (10)–(12) are the order parameters. As usual they can be introduced by referring to the Fourier expansion of $P^{(1)}(z,\uparrow)$, $P^{(1)}(z,\downarrow)$ or $P^{(1)}(z,s)$. Defining the expansion for $P^{(1)}(z,\uparrow)$ the corresponding expansions for $P^{(1)}(z,\downarrow)$ and $P^{(1)}(z,s)$ easily follow from Eqs. (8) and (12). For example, expanding $P^{(1)}(z,\uparrow)$ as

$$P^{(1)}(z,\uparrow) = \frac{1}{2} + 2\sum_{l=1} \tau_l \cos\left(\frac{2\pi l z}{d} + \psi_l\right) \tag{13}$$

the corresponding expansion for $P^{(1)}(z,s)$ is given by

$$P^{(1)}(z,s) = \frac{1}{2} + 2\sum_{l=1} \tau_l \cos\left(\frac{\pi l \Delta}{d}\right)\cos\left(\frac{2\pi l z}{d} + \frac{\pi l \Delta}{d} + \psi_l\right) + 2s\sum_{l=1} \tau_l \sin\left(\frac{\pi l \Delta}{d}\right)\sin\left(\frac{2\pi l z}{d} + \frac{\pi l \Delta}{d} + \psi_l\right), \tag{14}$$

where the smectic order parameters $\{\tau_l\}$ are averages over $P^{(1)}$:

$$\tau_l = \frac{1}{\overline{L_z}} \int_0^{\overline{L_z}} P^{(1)}(z,\uparrow) \cos\left(\frac{2\pi l z}{d} + \psi_l\right) dz \tag{15}$$

$$= \frac{1}{\overline{L_z}} \int_0^{\overline{L_z}} P^{(1)}(z,\downarrow) \cos\left(\frac{2\pi l (z+\Delta)}{d} + \psi_l\right) dz. \tag{16}$$

Here ψ_1 is an arbitrary phase reflecting freedom of choosing the origin of the system of frame; $\psi_l - \psi_1$ $(l>1)$ are the relative shifts between the harmonics and $0 \le \tau_l \le 1$. In addition to the purely translational order parameters, the τ_l, we identify the parameter Δ, which gives the average distance between the centers of mass of the molecules forming the two polarization waves within each smectic-A_d layer. The corresponding distance between the polarization planes is $2d_s - \Delta$. Note that introduction of Δ unifies description of smectic-A, smectic-A_d and smectic-A_2 phases. In the isotropic and nematic phases, $\tau_l = 0$ and Δ is undefined; in the smectic-A phase, $\tau_l \neq 0$, $\Delta = 0$; in the smectic-A_d phase of periodicity d, $\tau_l \neq 0$, $0 < \Delta < d/2$; in the smectic-A_2 or smectic-$\tilde{A}$, $\tau_l \neq 0$, $\Delta = d/2$. In the latter case, the expansion (14) becomes reduced to that studied in [14]. For perfect order all τ_l tend to unity. In order to distinguish between crystalline and the aforementioned smectic phases, we need to study, in addition, positional correlations perpendicular to the director using e.g. in-plane order parameters or transversal correlation functions [14].

Microscopic formulas for τ_l and Δ are easily inferred from simulations. For that we substitute the Fourier representation of the spatial Dirac delta function, $\delta(z - z_\alpha) = \sum_{n=-\infty}^{\infty} (1/\overline{L_z}) e^{i(2\pi n/\overline{L_z})(z - z_\alpha)}$, and the Kronecker delta representation, $\delta_{ss_\alpha} = \frac{1}{2}(1 + s s_\alpha)$, to Eq. (7). Observing that in constant-NPT MC simulations $\overline{L_z} = md$ and $n = ml$, we obtain a set of algebraic equations, which depend on τ_l, Δ, d and ψ_l:

$$\tau_l \cos\left(\frac{\pi l \Delta}{d}\right) e^{i\phi_l} = \left\langle \frac{1}{2N} \sum_{\alpha=1}^{N} e^{-i(2\pi l/d) z_\alpha} \right\rangle = c_l(d), \tag{17}$$

$$\tau_l \sin\left(\frac{\pi l \Delta}{d}\right) e^{i\tilde{\phi}_l} = \left\langle \frac{1}{2N} \sum_{\alpha=1}^{N} s_\alpha e^{-i(2\pi l/d) z_\alpha} \right\rangle = d_l(d), \tag{18}$$

where $\phi_l = \pi l \Delta / d + \psi_l$ and $\tilde{\phi}_l = \phi_l - \pi/2$.

There are three equivalent ways of determining d and the shift parameter Δ: Directly from positions of the peaks of the polarization waves; from positions of the peaks of the longitudinal (axial) pair distribution function introduced below and from maximization of $|c_1(d')|$ with respect to d'. All three methods give consistent results, which we present in Fig. 2. Interestingly, within stability range of the smectic-A_d phase, Fig. 8, both d and Δ are found within error to be temperature and pressure independent. Clearly, due to restrictions on position of the dipole moment d cannot exceed value of 5. With d so determined the equations (17) and (18) can be solved for τ_l and Δ to give $\tau_l = \sqrt{|c_l(d)|^2 + d_l(d)|^2}$ and $\sin(\pi l \Delta / d) = |d_l(d)| / \tau_l$. For the structures emerging from the simulations we evaluate only the leading, lowest order amplitude τ_1. Results along chosen isotherms are shown in Fig. 3. We also monitored layer formation with the help of longitudinal pair distribution functions, $g_\parallel^{(2)}(z, s_1 s_2)$. It gives the probability of finding two centers of mass of particles at a resolved, relative reduced distance of z along the director, and with orientations s_1, s_2 of the molecular dipoles relative to the same probability calculated for an ideal gas of particles at the same density. It reads [15]

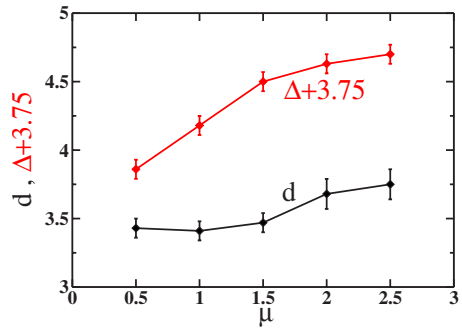

FIG. 2. (Color online) Layer spacing d along with Δ for stable smectic-A (A_d) islands of Fig. 8. Both parameters are within error temperature and pressure independent. The zero of Δ has been shifted by 3.75 on the vertical axis for clarity.

$$g_\parallel^{(2)}(z, s_1 s_2) = \frac{\overline{L_z}}{N^2} \left\langle \sum_i \sum_{j \neq i} \delta_{s_1 s_i} \delta_{s_2 s_j} \delta(z - |z_i - z_j|) \right\rangle. \tag{19}$$

Taking into account symmetry of the interaction potential we note that $g_\parallel^{(2)}$ must fulfill the condition that $g_\parallel^{(2)}(z, s_1 s_2) = g_\parallel^{(2)}(z, -s_1 - s_2)$. That is, only two functions, say

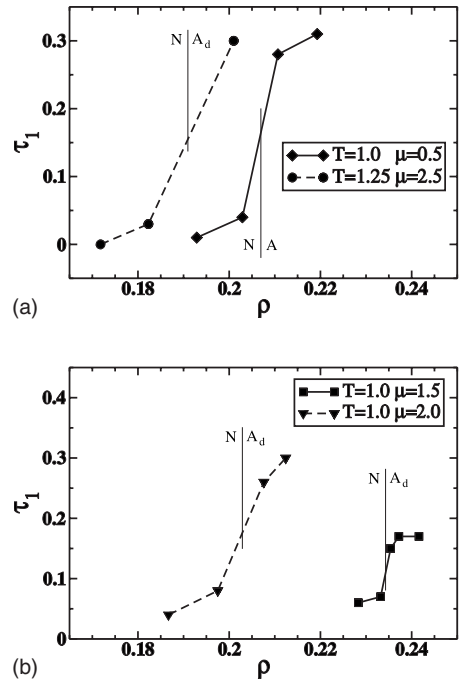

FIG. 3. Density variation of leading smectic order parameter τ_1 around nematic-smectic transition for exemplary isotherms $T = (1.0, 1.25)$ and dipole moments $\mu = (0.5, 1.5, 2.0, 2.5)$.

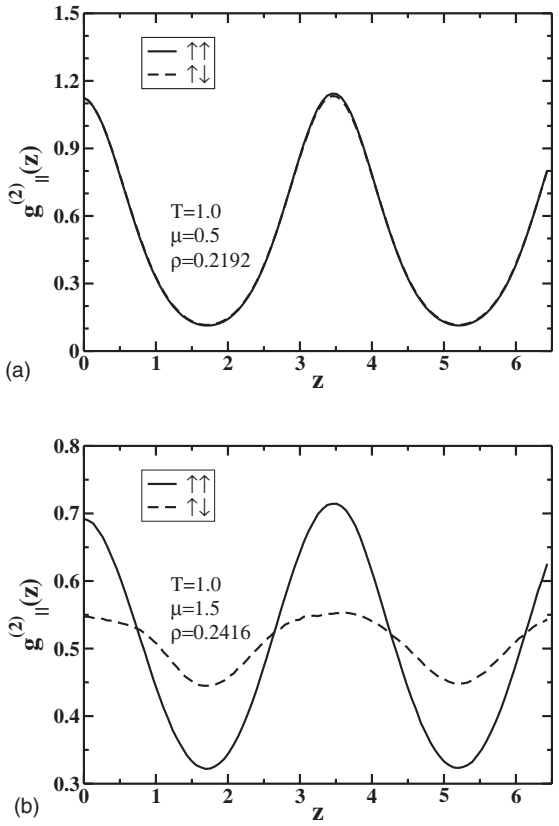

FIG. 4. Longitudinal pair distribution function measured along director (a) $T=1.0$, $\mu=0.5$, $\rho=0.2192$ and (b) $T=1.0$, $\mu=1.5$, $\rho=0.2416$. Absolute error in density does not exceed 0.0025.

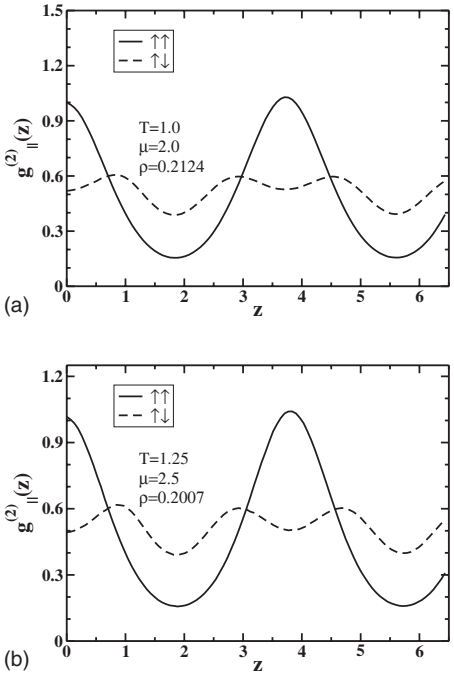

FIG. 5. Longitudinal pair distribution function measured along director (a) $T=1.0$, $\mu=2.0$, $\rho=0.2124$ and (b) $T=1.25$, $\mu=2.5$, $\rho=0.2007$. Absolute error in density does not exceed 0.0025.

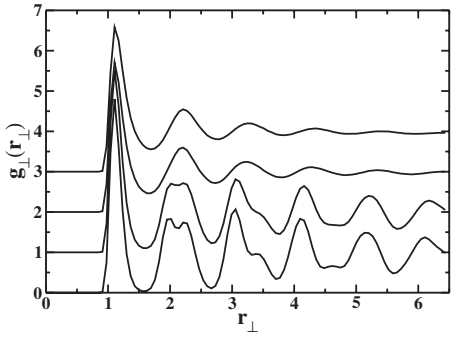

FIG. 6. Transversal pair correlation function $g_{\perp}^{(2)}(r_{\perp})$ as obtained from constant pressure MC simulations for system of 1000 polar GB molecules for $T=1.0$ isotherm and for $\mu=0.5$. Each curve corresponds, from top to bottom, to $\rho=0.2107$, 0.2192, 0.2325, and 0.2399 (with absolute error of 0.0025). The zero of $g_{\perp}^{(2)}(r_{\perp})$ has been shifted on the vertical scale for clarity.

$g_{\parallel}^{(2)}(z,\uparrow\uparrow)$ and $g_{\parallel}^{(2)}(z,\uparrow\downarrow)$ are independent. They are illustrated for selected thermodynamic states from smectic island in Fig. 4 and Fig. 5. For $\mu \lesssim 0.5$ only a monolayer smectic-A phase is stable ($\Delta=0$ within simulation error) with each layer containing, on the average, an equal number of molecules pointing "up" and "down." By contrast, the dipolar GB molecules with $\mu \gtrsim 0.5$ start to form an interdigitated smectic-A_d, Fig. 4, which is very well developed for $\mu \gtrsim 2$, Fig. 5.

The next step is to characterize positional correlations within each single layer. For that purpose we determined the in-layer transversal pair distribution function $g_{\perp}^{(2)}(r_{\perp})$, where $r_{\perp}$ is the separation between the centers of mass of particles projected onto a plane orthogonal to the director. It is defined as

$$g_{\perp}^{(2)}(r_{\perp}) = \frac{V}{4\pi r_{\perp} D N^2} \left\langle \sum_i \sum_{j \neq i} \delta(r_{\perp} - |\mathbf{r}_i - \mathbf{r}_j|_{\perp}) \times \Theta(D - |z_i - z_j|) \right\rangle, \tag{20}$$

where $D=0.2$ is a small parameter defining the layer's resolution. The correlation function (20) allows one to distinguish between liquidlike organization of the layers in the smectic-A (A_d) phase, with no positional long-range order and more ordered crystalline phases but our simulations made no distinction between quasi-long-ranged (hexatic) and true-long-ranged (crystalline) order. Therefore we collectively call "crystalline" all phases with nonliquid character of the layers. Figure 6 and Fig. 7 show behavior of $g_{\perp}^{(2)}$ for selected state points along the isotherms $T=1.0$ and $T=1.25$ for $\mu=0.5$ and $\mu=2.5$, respectively. Well resolved peaks for the in-plane correlations at high densities suggest that the ordered structures are crystalline ones.

Now, carrying out simulation and evaluating the order parameters and the pair distribution functions along isotherms we determined phase boundaries between liquid crystalline phases. Results are gathered in Fig. 8. Owing small hysteresis between isotropic and nematic, and between nematic and smectic-A_d phases, the corresponding phase boundaries approximate the liquid crystalline part of the phase diagrams

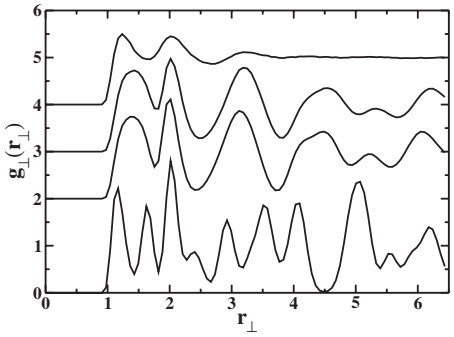

FIG. 7. Transversal pair correlation function $g_\perp^{(2)}(r_\perp)$ as obtained from constant pressure MC simulation for system of 1000 polar GB molecules for $T=1.25$ isotherm and for $\mu=2.5$. Each curve corresponds, from top to bottom, to $\rho=0.2007$, 0.2282, 0.2410, and 0.2624 (with absolute error of 0.0025). The zero of $g_\perp^{(2)}(r_\perp)$ has been shifted on the vertical scale for clarity.

quite accurately. Unfortunately, this is not the case for the transitions to- and from crystalline phases, especially for values of the dipole moment between 1.5 and 2.5, where quite considerable hysteresis has been observed. Recognizing this difficulty only the solid branch of the isotherm, obtained through expansion by slowly decreasing the input pressure (decompression) from a crystal structure at high pressure into liquid phases, is marked (triangles) on the diagrams. Consequently, the phase boundaries in Fig. 8 show where isotropic, nematic and smectic-A_d phases appear stable.

Figure 8(a)–8(f) show evolution of the liquid crystalline part of the phase diagram with increasing value of the dipole moment. It is clearly visible that the isotropic liquid-nematic coexistence line only weakly depends on the value of dipole moment. For $\mu \geq 1.5$ it moves slightly towards lower densities, but absolute changes do not exceed 6%. Similar feature was also observed by others for polar GB systems with dif-

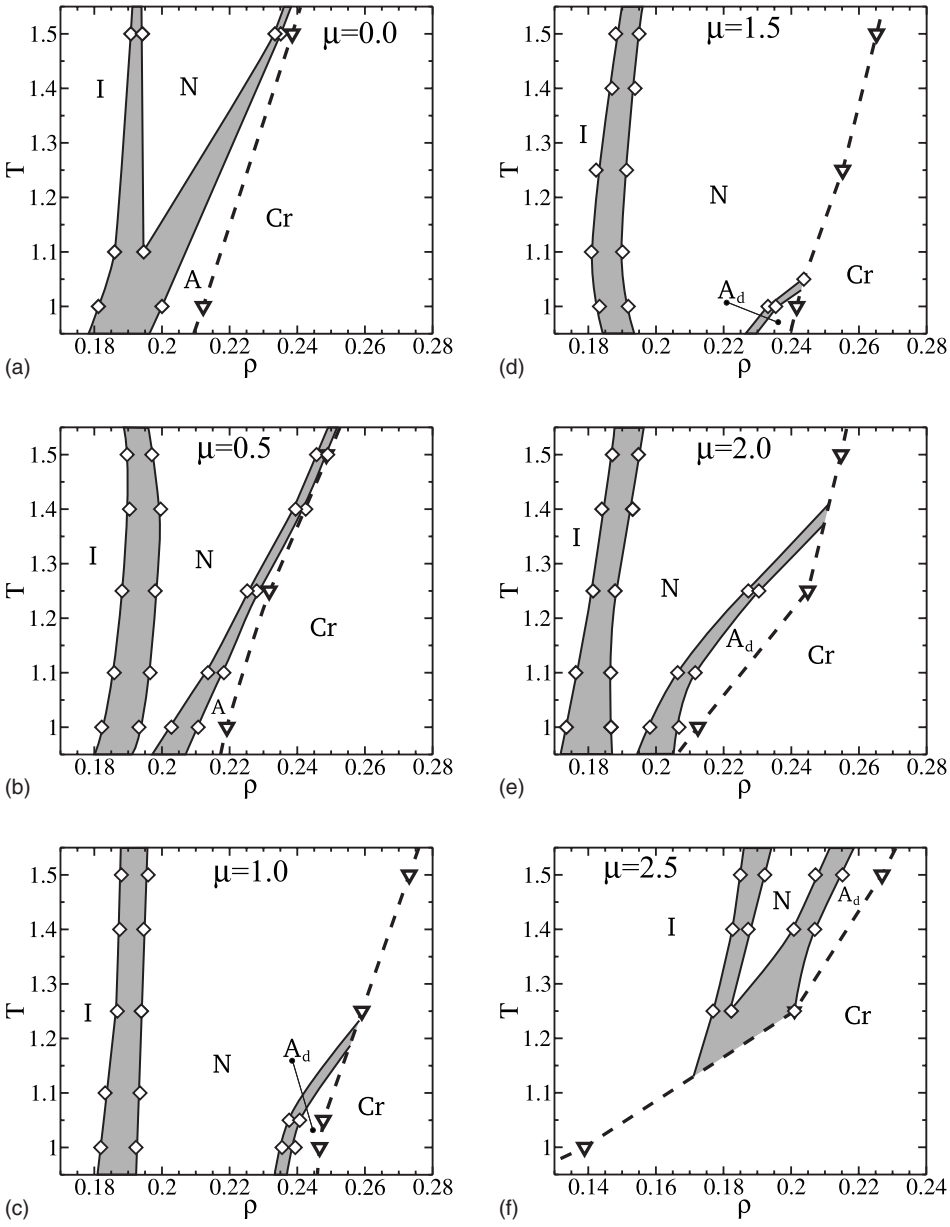

FIG. 8. Liquid crystalline part of phase diagram of polar GB fluids (diamonds) for six values of reduced dipole moment, obtained by slow increase or decrease of pressure along isotherms. Triangles denote stability limit of crystalline phases on decompression. *I* stands for isotropic, *N* for nematic, *A* for smectic *A*, A_d for smectic A_d, and *Cr* for "crystalline" phases. Lines are drawn to guide eye.

TABLE I. Ground states and corresponding lattice parameters as function of reduced dipole moment. Unit cell molecular configurations along with definitions of a, b, d, and Δ are shown in Fig. 9.

μ	Crystal system	Lattice parameters	
0.5	hexagonal AB stacking	$a=1.115$, $d=3.252$, $\Delta=0.00$	Fig. 9(a)
	(two ferroelectric biclinic sublattices)	$\rho=0.2859$	
1.0	monoclinic	$a=1.147$, $b=1.728$, $d=3.430$	Fig. 9(b)
	(two ferroelectric monoclinic sublattices)	$\Delta=0.96$, $\rho=0.2943$	
1.5	monoclinic	$a=1.151$, $b=1.687$, $d=3.525$	Fig. 9(b)
	(two ferroelectric monoclinic sublattices)	$\Delta=0.99$, $\rho=0.2923$	
2.0	monoclinic	$a=1.152$, $b=1.657$, $d=3.525$	Fig. 9(b)
	(two ferroelectric monoclinic sublattices)	$\Delta=0.99$, $\rho=0.2972$	
2.5	monoclinic	$a=1.189$, $b=1.622$, $d=3.665$	Fig. 9(b)
	(two ferroelectric monoclinic sublattices)	$\Delta=1.00$, $\rho=0.2830$	

ferent parameterizations, with central [14] and off-center [17] longitudinal dipoles.

By contrast, we observe strong influence of the dipole-dipole interaction on the smectic-A (A_d) part of the phase diagram. There are two characteristic threshold values for the dipole moment: $\mu_1 \approx 0.5$ and $\mu_2 \approx 1.5$-2, where features of the phase diagram change qualitatively. For $\mu \lesssim \mu_1$ we observe ordinary smectic-A phase, but when the dipole moment is greater than μ_1 the smectic-A phase converts into the smectic-A_d phase. With increasing dipole moment the nematic phase moves towards higher densities and expands at the expense of the smectic-A_d phase. In parallel, the temperature of isotropic-nematic-smectic triple point drops down. Both tendencies reverse when $\mu \gtrsim \mu_2$. As we demonstrate in the next section it is the in-layer structural reorganization enforced by frustration that causes these qualitative changes.

The effect of the dipole-dipole interaction on crystalline structures also is important for new structures emerge that do not exist in case of pure GB interactions. More systematically, in the limit of vanishing dipole the crystalline smectic-B phase (AB stacking), as observed by Brown *et al.* [12], is also confirmed by our simulations and appears stable down to $T=0$.

For nonzero dipole moments the ground states of the model show more possibilities, all being given in Table I and illustrated in Fig. 9. They are identified by a direct minimization of the interaction energy. In particular, for $\mu=0.5$ the ground state is identified with the hexagonal lattice (AB stacking) of dipoles forming ferroelectric lines [Fig. 9(a)]. The lines of opposite polarization interlace within each layer, which makes the net polarization of the layers vanish. The ferroelectric lines remain stable until $T<0.1$. For $T>0.1$ the dipoles prefer disordered configurations, but the long-range hexagonal order of the molecular centers of mass remains stable, i.e., the equilibrium crystalline structure is again similar to that observed for $\mu=0$. This dipole-disordered hexagonal structure was obtained both on compression and decompression along isotherms and emerged stable (compression) at $(T,\rho)=(1.0,0.2399)$ and $(T,\rho)=(1.25,0.2551)$. On decompression it disappeared for $(T,\rho)=(1.0,0.2192)$ and $(T,\rho)=(1.25,0.2317)$. Compression along $T=1.5$ isotherm did not show a distinct transition into a crystalline phase up to the highest simulation density of 0.2753.

For $\mu=1.0$ the ground state is a monoclinic lattice, Fig. 9(b), with the dipolar order of a single layer similar to that found for $\mu=0.5$, but ferroelectric sublayers do not belong to the same polar plane ($\Delta=0.96$). Positions of the three closest neighbors projected on the plane of a layer form an isosceles triangle, which becomes equilateral one in case of the hexagonal lattice for $\mu=0.5$. Under sufficiently high pressure and for all isotherms studied the monoclinic lattice transforms on decompression into hexagonal one (AB stacking) with dipolar disorder. The transformation takes place at $(T,\rho)=(1.0,0.2676)$, $(1.25,0.2755)$, and $(1.5,0.2813)$. The hexagonal structure has also been stabilized on compression, but only for $T=1.0$ isotherm; the corresponding reduced density reached value of 0.2674. For $T=1.25$ and $T=1.5$ the compression was stopped at $\rho=0.2835$ and $\rho=0.2747$, re-

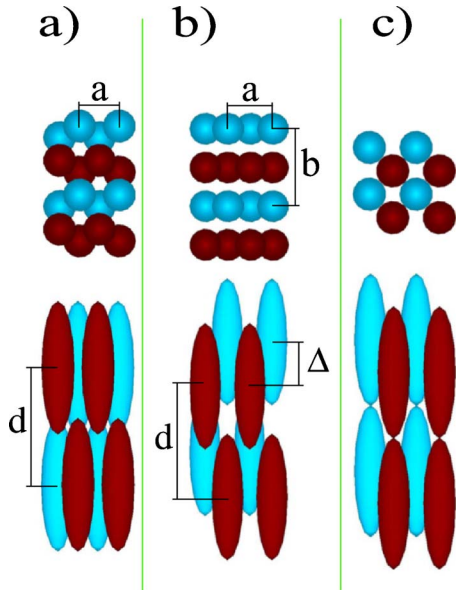

FIG. 9. (Color online) Ground state crystalline configurations obtained through a direct minimization of interaction energy and dipolar organization within sublayers: (a) Hexagonal crystal with AB stacking (top and side views); (b) monoclinic crystal; (c) antiferroelectric tetragonal ("square" in-plane) crystal, obtained for $\mu=2.5$ during compression of smectic-A_d and decompression of the monoclinic ground state crystal.

spectively, again without observing a distinct transition to crystalline phases.

In case of $\mu=1.5$ the system was compressed along isotherms: $T=1.0$, 1.25, and 1.5 up to reduced density of 0.2950 without having seen a distinct transition into crystal. Although a monoclinic structure eventually showed up at $T=0.7$ and $\rho=0.2838$ it was strongly perturbed by defects. As a result, the technique used allowed us to approximate the liquid crystal–crystal transition line by decompression only, which we performed starting from the ground state configurations.

For $\mu=2.0$ it was possible to compress the system into an ideal monoclinic crystal at $(T,\rho)=(1.0,0.2856)$, but along $T=1.25,1.5$ isotherms we again reached quite high density of 0.2950 without observing a transition into a crystalline phase. Finally, for $\mu=2.5$ the compression along $T=1.0,1.25$ isotherms led to the tetragonal, antiferroelectric crystal [Fig. 9(c)] at $\rho=0.2301$ and 0.2446, respectively, but no transition into crystal for $T=1.5$ has been confirmed up to the highest density studied ($\rho=0.2720$). Just as for smaller values of the dipole moment the ground state was identified with the monoclinic lattice. On decompression, it first transformed into the tetragonal (square-in plane) crystal at $(T,\rho)=(1.0,0.2305)$, $(1.25,0.2410)$, and next to liquid crystalline phases at lower densities. Along $T=1.5$ isotherm a monoclinic crystal transformed directly into the smectic-A_d phase.

IV. FINE STRUCTURE OF THREE-PARTICLE CORRELATIONS IN SMECTIC-A_d PHASE AND DIPOLAR FRUSTRATION

In the preceding section we showed that the evolution of liquid crystalline part of the phase diagram and the transformation of crystalline structures with increasing value of the dipole moment undergo qualitative changes close to the threshold value μ_2. Namely, for $\mu \lesssim \mu_2$ the nematic phase expands its area of stability at the expense of the smectic-A_d phase, while this tendency is reversed for the dipole moment larger than μ_2. In parallel, crystalline structures transform from hexagonal to monoclinic or tetragonal lattices. A purpose of this section is to show that this structural metamorphosis is induced by the dipolar frustration, which becomes so important for μ approaching μ_2 that the system prefers to change from frustrated hexagonal- to frustration-free tetragonal local order within each layer. As any frustrated configuration involves more than two molecules it prompts us to expect that a statistical description of the dipolar frustration requires study of, at least, three-particle correlations. Here we concentrate exclusively on three-particle correlations between positions of the dipoles. We should mention that already this limitation creates number of problems. One of them is a time consuming calculation of averages. For example, statistical average of a three-particle function in a system of $N=1000$ molecules requires analysis of $N(N-1)\times(N-2)/6=166167000$ triplet configurations in one cycle. Another difficulty is a graphical representation of the three-particle correlation functions.

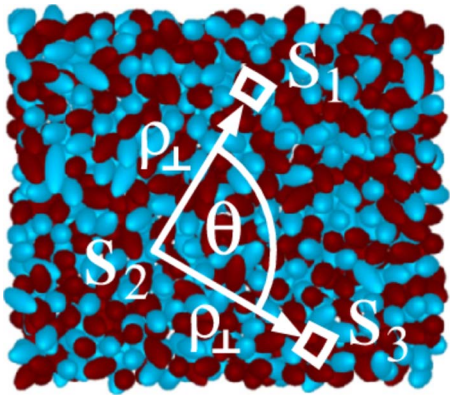

FIG. 10. (Color online) Parametrization of molecular configurations used to calculate transversal three-particle correlation function. Dark color denotes dipoles oriented up and light color corresponds to dipoles oriented down.

We solve these problems by introducing a three-particle transversal distribution function, which counts only these three dipoles that lay in planes perpendicular to the director and form isosceles triangles. Two sides of equal length $\rho_\perp$ of the triangle are assumed to form angle θ. Owing high orientational order in smectics we parameterize orientations using the discrete variables $\{s_i=\pm 1\}$ as introduced earlier for the pair distribution functions; details of the parametrization are shown in Fig. 10. The equilibrium structures emerging from simulations support a view that other configurations do not contribute in an essential way to quantitative understanding of the in-layer three-particle correlations. With these limitations the transversal three-particle distribution function between the dipole moments, expressed in cylindrical coordinates, reads [14,15]

$$g_\perp^{(3)}(\rho_\perp,\theta,s_1s_2s_3)=\frac{\bar{V}^2}{8\pi D^2N^3\rho_\perp^2}\times\left\langle\sum_i\sum_{j\neq i}\sum_{k\neq j\neq i}\delta_{s_1s_j}\delta_{s_2s_i}\delta_{s_3s_k}\delta(\rho_\perp-\rho_{\perp ji})\delta(\rho_\perp-\rho_{\perp ki})\Theta(D-|z_{ji}|)\Theta(D-|z_{ki}|)\hat{\Psi}(\theta,\phi_{ji},\phi_{ki})\right\rangle, \quad (21)$$

where $(\rho_{\perp ab},\phi_{ab},z_{ab})$ are the cylindrical coordinates of the relative distance $\boldsymbol{\rho}_{ab}=\boldsymbol{\rho}_a-\boldsymbol{\rho}_b$ between the dipoles a and b, Fig. 10. As previously $D=0.2$ is a small parameter defining resolution along the director. That is, the dipoles 1,2,3, Fig. 10, are associated with the same plane provided that $|z_a-z_2|<D$, $a=1,3$; $\hat{\Psi}(\theta,\phi_{ji},\phi_{ki})=1$ if the angle between arms $\rho_{\perp ji}$ and $\rho_{\perp ki}$ equals θ $(0\leq\theta<\pi)$ and $(\boldsymbol{\rho}_{ki}\times\boldsymbol{\rho}_{ji})\cdot\hat{\mathbf{z}}>0$, otherwise $\hat{\Psi}=\theta$. By definition, $g_\perp^{(3)}$ accounts for tendency of the three dipole moments to gather in polarization planes perpendicular to the director and shows what dipolar configurations are preferred within smectic and crystalline layers. For the model studied the isosceles configurations are most probable and, hence, bring important information about frustration. We distinguish between three nonequivalent di-

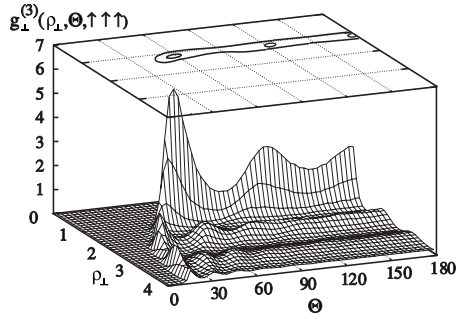

FIG. 11. Transversal, three-particle distribution function for $T=1.0$, $\mu=0.5$, $\rho=0.2107$ and $s_1s_2s_3=\uparrow\uparrow\uparrow$.

pole configurations: $s_1s_2s_3=\uparrow\uparrow\uparrow$, $\uparrow\uparrow\downarrow$ and $\downarrow\uparrow\downarrow$, and compute separately three distribution functions $g_\perp^{(3)}(\rho_\perp,\theta,\uparrow\uparrow\uparrow)$, $g_\perp^{(3)}(\rho_\perp,\theta,\uparrow\uparrow\downarrow)$ and $g_\perp^{(3)}(\rho_\perp,\theta,\downarrow\uparrow\downarrow)$, where the dipole moment s_2 refers to the nonequivalent vertex of the isosceles triangle, Fig. 10. The nonequivalent distribution functions are connected by the relation

$$g_\perp^{(3)}(\rho_\perp,\theta) \equiv \sum_{s_1,s_2,s_3} g_\perp^{(3)}(\rho_\perp,\theta,s_1s_2s_3)$$
$$= 2g_\perp^{(3)}(\rho_\perp,\theta,\uparrow\uparrow\uparrow) + 4g_\perp^{(3)}(\rho_\perp,\theta,\uparrow\uparrow\downarrow)$$
$$+ 2g_\perp^{(3)}(\rho_\perp,\theta,\downarrow\uparrow\downarrow), \qquad (22)$$

which follows from *global* up-down symmetry of pair interactions and symmetry with respect to exchange of s_1 and s_3 in Eq. (21). Please note that the exchange symmetry is not obeyed by the dipole s_2.

Applying the formula (21) to an ideal gas of molecules with density ρ yields normalization $N^{\text{ideal}}_{\rho_\perp\theta}=2\pi\delta\theta N(2\rho_\perp D\delta\rho_\perp\rho)^2$, where $N^{\text{ideal}}_{\rho_\perp\theta}$ is associated with the histogram element $(\rho_\perp,\rho_\perp+\delta\rho_\perp)$, $(\theta,\theta+\delta\theta)$. We compute $g_\perp^{(3)}(\rho_\perp,\theta)$ as $N_{\rho_\perp\theta}/N^{\text{ideal}}_{\rho_\perp\theta}$. As concerning technical aspects of the calculations we follow algorithm used by Mc Neil *et al.* [18].

Our analysis of the three-particle distribution functions is limited to smectic-*A* and smectic-A_d phases. We are mainly interested in evolution of the in-plane short-range order with increasing value of the dipole moment. For $\mu=0.5$ the molecules assume locally hexagonal ordering, which is evident from Fig. 11. The picture corresponds to the dominant dipolar configuration $s_1s_2s_3=\uparrow\uparrow\uparrow$. The remaining two functions, although look much the same, are an order of magnitude weaker but this relation between the probability amplitudes changes considerably as the dipole moment increases. In particular, the $s_1s_2s_3=\uparrow\uparrow\uparrow$ configurations appear practically irrelevant for $\mu\gtrsim 1.5$. For $\mu=2.5$, the weight of these configurations drops down by a factor of 10 as compared to the case with $\mu=0.5$. Increase of the dipole moment above $\mu\gtrsim 1.5$ causes the polarization planes to become dominated by the $s_1s_2s_3=\downarrow\uparrow\downarrow$ configurations. The dominance of the $g_\perp^{(3)}(\rho_\perp,\theta,\downarrow\uparrow\downarrow)$ distribution is correlated with a process of merging of the two polarization planes within each layer. Initially, they merge without giving up the short-range hexagonal order, which, in turn, sets in the dipolar frustration. As frustration gets stronger, for $\mu\approx 2.0$, an intermediate state is created, where $g_\perp^{(3)}(\rho_\perp,\theta,\downarrow\uparrow\downarrow)$ loses significantly its hexagonal character, Fig. 12. This is further observed in the shape of $g_\perp^{(3)}(\rho_\perp,\theta,\uparrow\uparrow\downarrow)$, Fig. 13, where the leading peak is due to equilateral triangle configurations for which $s_1s_2s_3=\downarrow\uparrow\downarrow$ and $s_1s_2s_3=\uparrow\uparrow\downarrow$ are equivalent. We interpret this intermediate state as being formed by antiferroelectrically correlated pairs of molecules, the "dimers." They break up, however, for sufficiently strong dipoles giving rise to the local tetragonal order as illustrated in Fig. 14 for $\mu=2.5$. Finally, we observe that when the local hexagonal order is transformed into the tetragonal one for $\mu\gtrsim 2.0$, the stability range of the smectic-A_d phase is enhanced at the expense of the nematic phase.

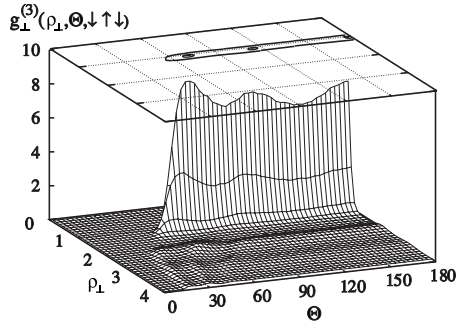

FIG. 12. Transversal three-particle distribution function for $T=1.0$, $\mu=2.0$, $\rho=0.2124$, and $s_1s_2s_3=\downarrow\uparrow\downarrow$.

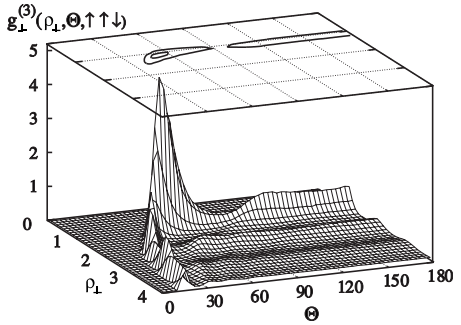

FIG. 13. Transversal three-particle distribution function for $T=1.0$, $\rho=0.2124$, $\mu=2.0$, and $s_1s_2s_3=\uparrow\uparrow\downarrow$.

V. FINAL CONCLUSIONS

We carried out *NPT* MC simulations for the GB molecules equipped with the off-center longitudinal dipole. The

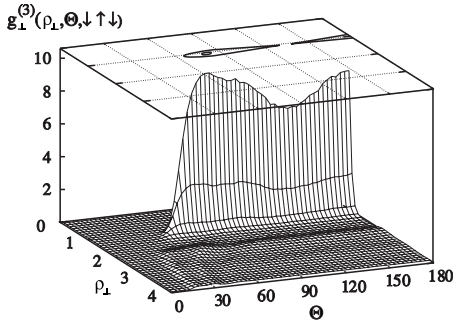

FIG. 14. Transversal three-particle distribution function for $T=1.25$, $\rho=0.2007$, $\mu=2.5$, and $s_1s_2s_3=\downarrow\uparrow\downarrow$.

phase diagram of the system and short range organization within smectic-A_d phase proved to be strongly dependent on the magnitude of the dipole moment. The isotropic-to-nematic phase transition was insensitive to weak and intermediate dipole moments whereas for stronger dipoles it moved towards lower densities. With regard to smectics the increasing dipole moment moves nematic-smectic coexistence line towards higher densities but after exceeding the threshold value of $\mu \approx 1.5$ this tendency reversed. For weak dipoles ($\mu \lesssim 0.5$) only the classical smectic-A phase with short-ranged hexagonal order was stabilized, which for stronger dipoles transformed into smectic-A_d with layers being formed by two ferroelectrically polarized sublayers of opposite polarization. For $\mu \lesssim 1.5$ each sublayer was also characterized by a short-range hexagonal order, but for sufficiently strong dipoles the system developed a competition between frustrated hexagonal- and frustration-free tetragonal local order within each layer. Studies of the three-particle distribution functions showed that due to this competition an intermediate, strongly frustrated state was created for $\mu \approx 2-2.5$, where the short-range ordering was almost devoid of any structure but ultimately the local tetragonal order won for sufficiently strong dipoles ($\mu \gtrsim 2.5$). Change of local hexagonal order into tetragonal one for $\mu \gtrsim 2.0$ enhanced stability of smectic-A_d at the expense of nematic. A similar competition was observed for crystalline phases between hexagonal, monoclinic and tetragonal orderings.

ACKNOWLEDGMENTS

This work was supported by Grant No. N202 169 31/3455 of Polish Ministry of Science and Higher Education, and by the EC Marie Curie Actions "Transfer of Knowledge," project *COCOS* (Contract No. MTKD-CT-2004-517186). We also gratefully acknowledge the computing grant G27-8 toward the use of the ICM (University of Warsaw) computers.

[1] G. H. Wannier, Phys. Rev. **79**, 357 (1950).
[2] See, e.g., A. P. Ramirez, Nature (London) **421**, 483 (2003).
[3] An excellent review is found in D. C. Wright and N. D. Mermin, Rev. Mod. Phys. **61**, 385 (1989); for recent research see, e.g., J. Englert, L. Longa, H. Stark, and H.-R. Trebin, Phys. Rev. Lett. **81**, 1457 (1998); J. Englert, H. Stark, L. Longa, and H. R. Trebin, Phys. Rev. E **61**, 2759 (2000); L. Longa, M. Ciesla, and H.-R. Trebin, *ibid.* **67**, 061705 (2003); E. Grelet, B. Pansu, M. H. Li, and H. T. Nguyen, Phys. Rev. Lett. **86**, 3791 (2001); B. A. DiDonna and R. D. Kamien, *ibid.* **89**, 215504 (2002).
[4] P. E. Cladis, Phys. Rev. Lett. **35**, 48 (1975); G. Sigaud, F. Hardouin, M. F. Achard, and H. Gasparoux, J. Phys. Colloq. **40**, C3-356 (1979); A. M. Levelut, R. J. Tarento, F. Hardouin, M. F. Achard, and G. Sigaud, Phys. Rev. A **24**, 2180 (1981); F. Hardouin, Physica A **140**, 359 (1986); J. Prost and P. Barois, J. Chim. Phys. Phys.-Chim. Biol. **80**, 65 (1983).
[5] C. Vega and S. Lago, J. Chem. Phys. **56**, 6727 (1994); A. G. Vanakaras and D. J. Photinos, Mol. Phys. **85**, 1089 (1995).
[6] D. C. Williamson and F. del Rio, J. Chem. Phys. **107**, 9549 (1997).
[7] A. N. Berker and J. S. Walker, Phys. Rev. Lett. **47**, 1469 (1981); L. Longa and W. H. de Jeu, Phys. Rev. A **26**, 1632 (1982); **28**, 2380 (1983); L. Longa, "Models of high-temperature liquid crystalline phases and of related phase transitions," Institute of Nuclear Physics, Kraków, Poland, Report No 1454/PH, 1989.
[8] J. G. Gay and B. J. Berne, J. Chem. Phys. **74**, 3316 (1981).
[9] E. de Miguel and C. Vega, J. Chem. Phys. **117**, 6313 (2002); E. de Miguel, Mol. Phys. **100**, 2449 (2002); E. de Miguel, E. M. del Río, and F. J. Blas, J. Chem. Phys. **121**, 11183 (2004); E. de Miguel, E. M. del Río, J. T. Brown, and M. P. Allen, *ibid.* **105**, 4234 (1996).
[10] R. Berardi, A. P. J. Emerson, and C. Zannoni, J. Chem. Soc., Faraday Trans. **89**, 4069 (1993).
[11] M. A. Bates and G. R. Luckhurst, J. Chem. Phys. **110**, 7087 (1999).
[12] J. T. Brown, M. P. Allen, E. Martin del Río, and E. de Miguel, Phys. Rev. E **57**, 6685 (1998).
[13] W. Jozefowicz, G. Cholewiak, and L. Longa, Phys. Rev. E **71**, 032701 (2005).
[14] For a review of simulations of dipolar Gay-Berne systems, see L. Longa, H.-R. Trebin, and G. Cholewiak, in *Relaxation Phenomena: Liquid Crystals, Magnetic Systems, Polymers, High-Tc Superconductors, Metallic Glasses*, edited by W. Haase and S. Wróbel (Springer-Verlag, Heidelberg, 2003), pp. 204–233.
[15] L. Longa, G. Cholewiak, and J. Stelzer, Acta Phys. Pol. B **31**, 801 (2000).
[16] R. Berardi, S. Orlandi, and C. Zannoni, Chem. Phys. Lett. **261**, 357 (1996).
[17] R. Berardi, S. Orlandi, D. J. Photinos, A. G. Vanakaras, and C. Zannoni, Phys. Chem. Chem. Phys. **4**, 770 (2002).
[18] W. J. McNeil, W. G. Madden, A. D. J. Haymet, and S. A. Rice, J. Chem. Phys. **78**, 388 (1983); M. Fushiki, Mol. Phys. **44**, 307 (1991).
[19] M. P. Allen and D. J. Tildesly, *Computer Simulation of Liquids* (Clarendon, Oxford, 1987).
[20] M. Houssa, A. Oualid, and L. F. Rull, Mol. Phys. **94**, 439 (1998).
[21] B. Garzón, S. Lago, and C. Vega, Chem. Phys. Lett. **231**, 366 (1994).
[22] G. Cholewiak, Ph.D. thesis, Jagellonian University, M. Smoluchowski Institute of Physics, Kraków, 2002.
[23] A. Gil-Villegas, S. C. McGrother, and G. Jackson, Mol. Phys. **92**, 723 (1997)